

## Hydrogen and Defects in Amorphous Silicon

Sufi Zafar<sup>(a)</sup> and E. A. Schiff

Physics Department, Syracuse University, Syracuse, New York 13244-1130

(Received 13 August 1990)

Experimental evidence for two regimes in the relationship of the defect density to the hydrogenation state of hydrogenated amorphous silicon (*a*-Si:H) is presented. A previous model for the defect density based on the two phases of bound hydrogen in *a*-Si:H is shown to account for the measured relationship.

PACS numbers: 61.42.+h, 71.55.Ht, 76.30.Mi

The incorporation of hydrogen in amorphous silicon is associated with a remarkable improvement in its properties, and has led to the widespread applications of this material. One signature of this improvement is the reduction in the density of paramagnetic defects or *D* centers measured by electron-spin resonance from about  $10^{19} \text{ cm}^{-3}$  in elemental amorphous silicon (*a*-Si) to as few as  $10^{15} \text{ cm}^{-3}$  in hydrogenated amorphous silicon (*a*-Si:H). Since the discovery of *a*-Si:H about fifteen years<sup>1</sup> ago, a fairly complete picture of the hydrogen in *a*-Si:H has emerged, primarily from nuclear-magnetic-resonance<sup>2,3</sup> and infrared-absorption measurements.<sup>4</sup> However, the relationship between this hydrogen and the defects which remain in the material is unclear. One of the most successful recent models for defects in *a*-Si:H does not explicitly involve hydrogen at all. This "defect-pool" model<sup>5</sup> accounts for the density of *D* centers by assuming that they can interconvert with states near the top of the valence band. These bandtail states can be detected by optical measurements, and the model accounts well for the correlation of the measurements with the *D*-center density as well as for the temperature dependence of this density.<sup>5-7</sup> Despite its successes, in an important sense this model is provisional: Microscopic structures for the bandtail states and the *D* center are not specified.

In this Letter we develop a perspective on the defect density in *a*-Si:H based exclusively on its hydrogen microstructure. We first propose a phenomenological relationship between hydrogen and the density of *D* centers (the "spin density"). This proposal is based on several recent measurements, some of which will be reported here. We find distinct low- and high-spin-density regimes; the relationship is sufficiently detailed that it provides a serious test for defect models. We then show that a previously published model relating the spin density to the two principal hydrogen microstructures<sup>8</sup> of *a*-Si:H accounts for the two regimes in detail. The proposed defect-hydrogen relationship also has important consequences for the defect densities produced by deposition and by illumination in *a*-Si:H which will be briefly described at the conclusion of this Letter.

We commence by discussing the deuteration measurements of Jackson, Tsai, and Thompson,<sup>9</sup> which can be

reinterpreted to yield a relationship between the hydrogen and spin densities in *a*-Si:H. These authors studied *a*-Si:H specimens which were depleted of hydrogen by heating them to  $555^\circ\text{C}$  and then deuterated by exposure to deuterium plasmas at several temperatures. The resulting spin and deuterium density profiles were then measured at room temperature.

The inset of Fig. 1 shows a deuterium profile for  $350^\circ\text{C}$  deuteration. We analyzed the deuterium profiles to obtain what we shall term the *hydrogen-deficit* profile  $\tilde{H}(x)$  of the specimen. The relatively large density of deuterium near the surface presumably corresponds to complete hydrogenation of the available hydrogen bonding sites. Prior to deuteration the depleted specimens

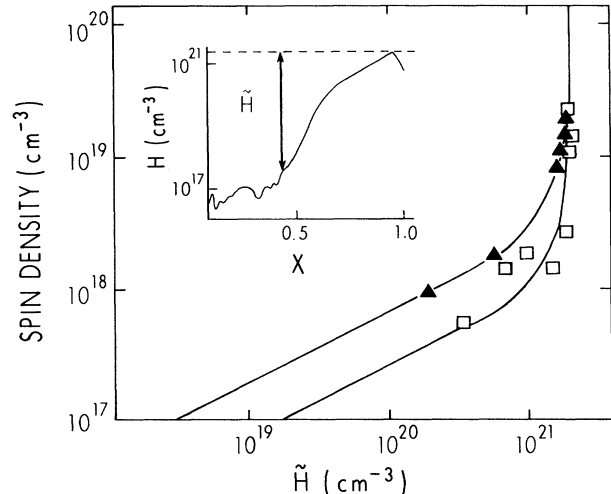


FIG. 1. Measured and calculated dependence of the spin density upon hydrogen deficit  $\tilde{H}$  (density of unoccupied hydrogen-bonding sites) in *a*-Si:H. Measured points are based on spin density and deuterium profiles reported by Jackson, Tsai, and Thompson (Ref. 9) in specimens which were first depleted of hydrogen and then plasma deuterated.  $\tilde{H}$  was estimated as shown in the inset from the measured deuterium density profiles. Symbols indicate  $350^\circ\text{C}$  ( $\Delta$ ) and  $400^\circ\text{C}$  ( $\square$ ) deuteration. The calculations using a hydrogen-deficit model (Ref. 8) are at temperatures of  $250^\circ\text{C}$  (upper curve) and  $200^\circ\text{C}$  (lower curve). Note the apparently asymptotic behavior for deficits approaching  $2 \times 10^{21} \text{ cm}^{-3}$ .

therefore had a deficit of about  $2 \times 10^{21} \text{ cm}^{-3}$  (the maximum value of the deuterium density). In the deuterated specimen the deficit increases from essentially zero near the surface to nearly its initial value deeper inside; the conversion of the measured deuterium profile to a deficit profile is illustrated by the arrow in the inset.

In Fig. 1 we have plotted the correlation of the hydrogen deficits at different depths of a specimen with the spin-density values  $N_s(x)$  measured at the same depths. The results for deuteration at 350 and at 400 °C are shown. A third pair of profiles for 450 °C deuteration were essentially flat and are not shown. The solid lines are calculations which will be discussed subsequently.

For smaller hydrogen deficits the data suggest a sub-linear dependence of the spin density upon hydrogen deficit; when the spin density is  $3 \times 10^{18} \text{ cm}^{-3}$ , the hydrogen deficit is about 3 orders of magnitude larger. The sublinearity and the large discrepancy between the deficit and the spin density are consistent with earlier measurements of the correlation between the increase in the spin density and the volume of hydrogen evolved from  $a\text{-Si:H}$  during high-temperature treatments;<sup>10</sup> the earlier data suggest essentially a square-root dependence of spin density upon deficit which is not apparent in Fig. 1. The data of Fig. 1 also show an "asymptotic" increase in spin density at  $\bar{H} = 2 \times 10^{21} \text{ cm}^{-3}$  which has not, to our knowledge, been noticed before. Since the total hydrogen content of  $a\text{-Si:H}$  when deposited is typically  $4 \times 10^{21} \text{ cm}^{-3}$ ,<sup>2,3</sup> this asymptote apparently reflects a change in behavior near the onset of complete dehydrogenation of the specimen.

In addition to its dependence upon hydrogen deficit, the spin density in  $a\text{-Si:H}$  depends on the specimen's temperature.<sup>5-7,11</sup> In Fig. 2 we reproduce as the open symbols some published data<sup>11</sup> from our laboratory showing this effect in a variety of as-deposited specimens; the straight lines in this figure correspond to a thermally activated form of the temperature dependence. We have now also measured this temperature dependence in the "asymptotic" regime by using hydrogen-depleted specimens. These new results are presented as the solid symbols in Fig. 2. The lower curve corresponds to the as-deposited state, and the two upper curves to hydrogen-depleted states obtained by annealing at 500 and 550 °C for several hours. The depleted specimens have distinctly smaller thermal-activation energies.

We checked that the states displayed in Fig. 2 corresponded to spatially homogeneous spin densities by using a series of four specimens with thicknesses varying between 0.5 and 5.0  $\mu\text{m}$ . Additional states for which the average spin density depended upon thickness were not included in Fig. 2. In addition, we measured the "equilibration" times for each state as a function of temperature; this time characterizes the rate at which the spin density achieved its equilibrium value following temperature changes. For all three states we found thermally ac-

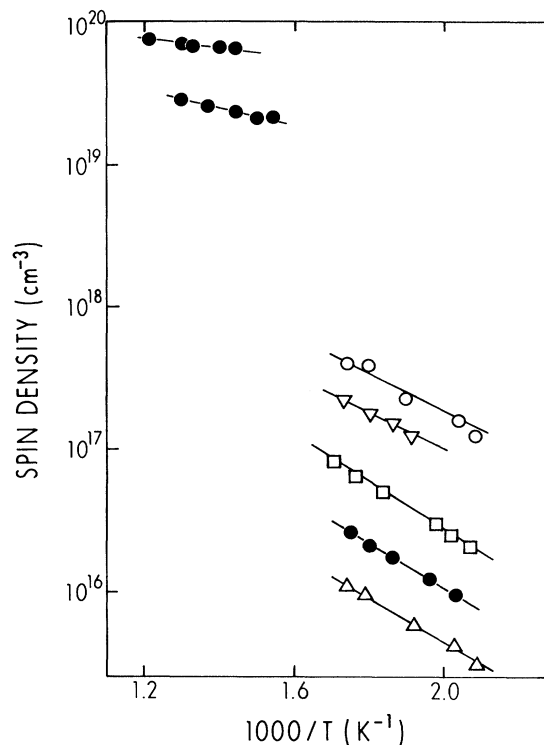


FIG. 2. Measured spin density as a function of temperature for several samples in  $a\text{-Si:H}$ . The solid symbols represent spin-density estimates for three hydrogenation states: as-deposited (lower curve) and hydrogen depleted (upper curves). Open symbols represent spin densities for as-deposited states of additional specimens (Ref. 11). The solid lines were used to estimate thermal-activation energies.

tivated equilibration with an activation energy of 1.6 eV, which is comparable to the hydrogen diffusion activation energy in  $a\text{-Si:H}$ .<sup>12</sup>

In Fig. 3 we have correlated the activation energies estimated from Fig. 2 with the spin density at 350 °C extrapolated from the activated behavior; the two error bars shown represent the reproducibility of the activation energy in independent measurements on a given specimen. The solid line represents a calculation which will be discussed shortly. It is clear that the activation energy is reasonably independent of specimen conditions for the as-deposited specimens (points with spin densities less than  $10^{18} \text{ cm}^{-3}$ ), and that the two hydrogen-depleted specimens (spin densities exceeding  $10^{19} \text{ cm}^{-3}$ ) show markedly reduced activation energies.

We propose the following two-regime relationship of hydrogen to the spin density in  $a\text{-Si:H}$  based on the measurements of Figs. 1-3. For lower spin densities ( $< 10^{18} \text{ cm}^{-3}$  near 350 °C) the spin density depends sublinearly upon hydrogen deficit, and the thermal-activation energy (about 0.3 eV) of the spin density is essentially independent of deficit. For larger spin densities the dependence

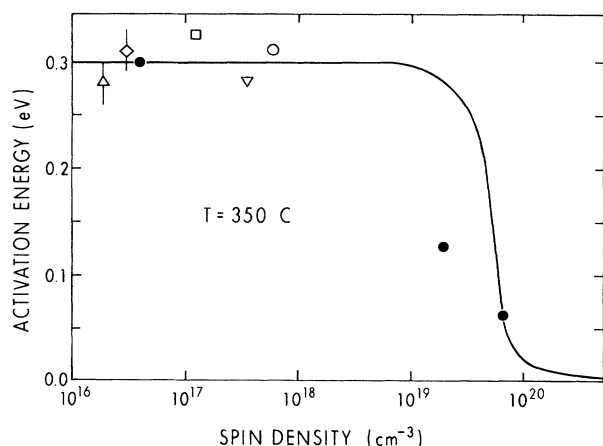


FIG. 3. The dependence of the thermal-activation energy of the spin density upon the spin density itself for  $a$ -Si:H at 350°C. The points are based on the measurements reported in Fig. 2 and use the same symbols. The solid line represents a calculation using the hydrogen-deficit model. Note the loss of thermal activation in hydrogen-depleted specimens (solid symbols at the right of the figure).

of the spin density upon further changes in hydrogen deficit is much steeper, and activated behavior of the spin density is essentially lost.

We now discuss the implications of this relationship for defect models of  $a$ -Si:H. Models based primarily upon bandtail states<sup>5</sup> or electric-potential fluctuations<sup>13</sup> cannot directly address the hydrogen-deficit relationship of Fig. 1. In principle, these models should account for the relationship of Fig. 3, but we shall not discuss this here. Of the several hydrogen-based models,<sup>8,14-16</sup> only one was developed to accommodate the type of thermal equilibrium data of Figs. 1-3. This model appears to offer a satisfactory account of the data; calculations based on this model were presented as the solid lines in Figs. 1 and 3. In the remainder of this Letter we briefly describe these calculations.

We shall refer to this model as a *hydrogen-deficit* model. It was based on the microstructure for  $a$ -Si:H suggested by the two phases of hydrogen observed by NMR.<sup>2,3</sup> One phase consists of clusters of about six hydrogen atoms in close proximity; the second consists of dilute hydrogen atoms spatially isolated from other hydrogen. Each phase typically contains  $2 \times 10^{21} \text{ cm}^{-3}$  hydrogen atoms. Infrared vibrational spectroscopy indicates that essentially all this hydrogen is bound to Si atoms, apparently as *monohydrides* in electronic quality  $a$ -Si:H.<sup>4</sup> The underlying silicon microstructure therefore contains two principal types of sites which bond hydrogen, corresponding to the observed clustered and dilute phases. Hydrogen in other environments was neglected.

The hydrogen-deficit model assumed that the spins observed in  $a$ -Si:H are due to unhydrogenated sites on the dilute phase—even if much larger densities of sites on

the clustered phase are also unhydrogenated. These latter sites were assumed to be spinless “weak bonds.” The neglect of spins on the clustered phase was justified on the basis that weak bonds tend to bind *pairs* of hydrogen atoms instead of single atoms.<sup>8,15,17</sup>

The partition functions required to calculate the dependence of the equilibrium spin density upon temperature and hydrogenation state were given in Ref. 8. The three numerical parameters required are the densities of sites in each phase ( $N_C$  and  $N_D$ ) and the difference  $\delta E$  in the mean binding energy of hydrogen atoms on the phases. Site densities were estimated from NMR measurements; we used a typical value of  $2 \times 10^{21} \text{ cm}^{-3}$  for the maximum density of hydrogen bonded to the clustered and also to the dilute phase.<sup>2,3</sup> The binding-energy difference  $\delta E$  can be equated to the thermal-activation energy of the spin density in the limit of low densities.<sup>8</sup> We used the value of 0.3 eV suggested by Fig. 3; the sign of  $\delta E$  indicates that the mean binding energy for hydrogen on the clustered phase is smaller than on the dilute phase. We then evaluated the spin density in this model as a function of temperature and hydrogen deficit (the density of hydrogen “missing” from the two phases) using standard numerical procedures.

In Fig. 1 we presented measurements of the dependence of the spin density upon the hydrogen deficit for two deuteration temperatures. The solid lines are the calculated dependence of the equilibrium spin density upon the hydrogen deficit at 200 and 250°C. Each calculated curve shows two regimes. For smaller spin densities there is a square-root dependence of the spin density upon hydrogen deficit and a large ratio of the deficit to the spin density. The spin density then increases “asymptotically” as the hydrogen deficit approaches  $2 \times 10^{21} \text{ cm}^{-3}$ . In the square-root regime most unhydrogenated sites are on the clustered phase, since for  $\delta E = 0.3 \text{ eV}$  hydrogen is more weakly bound to this phase than to the dilute phase. The spin density is due only to the relatively small density of unhydrogenated sites on the dilute phase, and is thus much smaller than the deficit. The second “asymptotic regime” occurs when the clustered phase is depleted of hydrogen; in this latter regime any further increase in the deficit corresponds to removal of hydrogen from the dilute phase. Each hydrogen removed leaves a spin, thereby leading to the rapid rise in spin density.

The measurements shown in Fig. 1 have the same behavior as a function of hydrogen deficit predicted by this model, and the hydrogen deficit of  $2 \times 10^{21} \text{ cm}^{-3}$  at the asymptote was also as predicted. However, the curves shown in this figure were calculated at temperatures lower than the experimental deuteration temperatures; calculations at the deuteration temperatures yielded spin densities about 3 (at 350°C) or 5 (at 400°C) times higher than the measured densities. We shall not discuss possible refinements of the analysis or experimental pro-

cedure which might have reduced this difference, instead noting that the form and magnitude of the measurements are surprisingly well reproduced by the model *without any adjustments based on the data*.

In Fig. 3 we presented measurements of the spin-density activation energy as a function of the magnitude of the spin density near 350 °C. The solid line presents the related calculation; there are again two regimes. For low spin densities the spin density is thermally activated. In the model, raising the specimen's temperature transfers hydrogen from dilute phase sites to the empty clustered phase sites, leaving spins behind on the dilute phase. As for Fig. 1, at higher spin densities the clustered phase is depleted of hydrogen. In this regime the spin density is not activated.

The data for as-deposited specimens in Fig. 3 (spin densities less than  $10^{18} \text{ cm}^{-3}$ ) are rationalized in terms of the hydrogen-deficit model by assuming that the various specimens have comparable values for  $\delta E$  and varying hydrogen deficits. The data for the two hydrogen-depleted states (rightmost solid symbols) directly verify the prediction of the model that depletion of the clustered phase will lead to nonactivated dependence of the spin density.

We believe that the substantial agreement of measurement and calculation summarized in Figs. 1 and 3 establishes that the thermal equilibrium spin density in *a*-Si:H is determined by the distribution of hydrogen on the two-phase microstructure of this material revealed by NMR. This view has important consequences for other defect phenomena. First, we suggest that differences in the defect densities of as-deposited specimens primarily reflect differences in their hydrogen deficits. Changes in microstructure parameters (the densities of clustered and dilute phase sites for the model used here) would be of secondary importance. We are unaware of any research into the relationship of the deficit and deposition parameters.

The second phenomenon is the creation of metastable spins by illumination or other excess carrier processes. One recent model for metastability proposed by Zhang, Jackson, and Chadi<sup>16</sup> envisioned spin creation via dissociation of hydrogen pairs in " $\text{H}_2^+$ " complexes. This mechanism is essentially reversed from the mechanism

used here to compute the dependence of the spin density upon temperature, which involved spin creation via association of pairs of hydrogen on clustered phase sites. The apparent contradiction reveals the important role which the equilibrium hydrogen-defect relationship we have described in Figs. 1–3 can play in formulating metastability models; in our view models which do not accommodate the equilibrium measurements can most probably be excluded.

This work was supported by SERI XB-6-06005-2.

<sup>1</sup>W. E. Spear and P. G. Le Comber, *Solid State Commun.* **17**, 1193 (1975).

<sup>2</sup>J. C. Knights, in *The Physics of Hydrogenated Amorphous Silicon I*, edited by J. D. Joannopoulos and G. Lucovsky (Springer-Verlag, Berlin, 1984), p. 5.

<sup>3</sup>J. Baum, K. K. Gleason, A. Pines, A. N. Garroway, and J. A. Reimer, *Phys. Rev. Lett.* **56**, 1377 (1986).

<sup>4</sup>G. Lucovsky and W. B. Pollard, in *The Physics of Hydrogenated Amorphous Silicon II*, edited by J. D. Joannopoulos and G. Lucovsky (Springer-Verlag, Berlin, 1984), p. 301.

<sup>5</sup>Z. E. Smith and S. Wagner, in *Amorphous Silicon and Related Materials*, edited by H. Fritzsche (World Scientific, Singapore, 1988), p. 409.

<sup>6</sup>X. Xu, A. Okumura, A. Morimoto, M. Kumeda, and T. Shimizu, *Phys. Rev. B* **38**, 8371 (1988).

<sup>7</sup>R. A. Street and K. Winer, *Phys. Rev. B* **40**, 6236 (1989).

<sup>8</sup>Sufi Zafar and E. A. Schiff, *Phys. Rev. B* **40**, 5235 (1989).

<sup>9</sup>W. B. Jackson, C. C. Tsai, and R. Thompson, *Phys. Rev. Lett.* **64**, 56 (1990).

<sup>10</sup>D. K. Biegelsen, R. A. Street, C. C. Tsai, and J. C. Knights, *Phys. Rev. B* **20**, 4839 (1979).

<sup>11</sup>Sufi Zafar and E. A. Schiff, *J. Non-Cryst. Solids* **114**, 618 (1989).

<sup>12</sup>D. E. Carlson and C. W. Magee, *Appl. Phys. Lett.* **33**, 81 (1978).

<sup>13</sup>Howard M. Branz and Marvin Silver, *Phys. Rev. B* **42**, 7420 (1990).

<sup>14</sup>W. B. Jackson and J. Kakalios, in *Amorphous Silicon and Related Materials* (Ref. 5), p. 247.

<sup>15</sup>R. A. Street, M. Hack, and W. B. Jackson, *Phys. Rev. B* **35**, 4209 (1988).

<sup>16</sup>S. B. Zhang, W. B. Jackson, and D. J. Chadi, *Phys. Rev. Lett.* **65**, 2575 (1990).

<sup>17</sup>M. E. Eberhart, K. H. Johnson, and D. Adler, *Phys. Rev. B* **26**, 3138 (1982).